

Preparation and Characterization of Rutile-Type TiO₂ Doped with Cu

B. Tryba, J. Orlikowski, R.J. Wróbel, J. Przepiórski, and A.W. Morawski

(Submitted May 15, 2014; in revised form January 15, 2015; published online January 30, 2015)

Visible-light active photocatalysts were prepared by doping Cu-TiO₂ through the sol-gel method. The influence of the preparation conditions such as pH of sol-gel solution and calcination temperature on the properties of TiO₂-Cu was investigated. The presence of Cu caused reduction of band-gap energy, which was more visible in the rutile-type TiO₂. Low pH of sol-gel solution such as pH 1.5 favored formation of rutile during calcination and caused slower growth of the crystallites with increasing temperature of calcination in comparison with sol-gel prepared at pH 3. XPS measurements showed that Cu was placed mostly on the surface of TiO₂. For sample calcined at 600 °C, the surface concentration of copper was 1.1 wt.%. The presence of both, rutile phase and Cu, increased adsorption of phenol and facilitated its photocatalytic decomposition. Moreover, reduced band-gap energy in rutile-type TiO₂-Cu photocatalyst enabled phenol decomposition under visible light.

Keywords phenol mineralization, rutile-type TiO₂, sol-gel, visible-light activity

1. Introduction

TiO₂ has been widely studied in the literature due to its several good properties, such as low cost, nontoxicity, physical and chemical stability, and high photocatalytic activity (Ref 1, 2). Because of these excellent properties, TiO₂ has become one of the most commonly used photocatalysts in the photodegradation of pollutants in both media, water and air (Ref 3-5). However, TiO₂ has the wide band-gap energy that limits its application in the visible range (Ref 6-8). Therefore, many studies have been performed to extend the light absorption of TiO₂ from UV to visible light, in order to extend its photocatalytic properties. For this purpose, doping of impurities or different surface modifications are commonly used (Ref 9-12). Particularly, metals and non-metals doping has been widely studied in TiO₂ synthesis by sol-gel method (Ref 13-16). For example, copper as a metal dopant in TiO₂ can form an additional band. According to Guo and Du (Ref 17), Cu doping to TiO₂ can induce some doping states near the top of valance band, and thus, both enhance the visible absorption in the range of 400-1000 nm by Cu 3d-Ti 3d optical transition and extend the recombination pathway of e⁻/h⁺ pair. However, conditions of the sol-gel synthesis as well as heat treatment temperature play an important role in incorporation of Cu to the TiO₂ lattice (Ref 18). These preparation conditions determine position of dopant in TiO₂ structure and as a consequence conduct to the different activities of TiO₂. Therefore, the copper dopant can influence on the formation of phase composition as well as crystallites of TiO₂.

Sahu et al. (Ref 19) reported that increasing the copper dopant concentration promotes an anatase to rutile phase transformation, decreased crystalline nature, and primary particle size.

On the other hand, another factors like sort of used Cu and TiO₂ precursors, pH of sol-gel solution, and calcination temperature can be also considered as the crucial factors influencing on the properties of the final TiO₂ photocatalyst. It has been proved that the properties of the final product depend on both, TiO₂ and copper precursors, used for sol-gel synthesis (Ref 20-23). The TiO₂ precursors like titanium isopropoxide (TIP), titanium tetrachloride (Ref 24-26), and copper precursors like CuSO₄, CuCl₂, and Cu(NO₃)₂ (Ref 27-29) can be successfully used for this purpose. Additionally, it was found that sol-gel synthesis carried out at pH about 3 resulted in the most photoactive final product (Ref 30, 31). However, at the stronger acid conditions, the reverse effect of the photocatalytic activity of TiO₂ was observed. It is commonly known that calcination temperature also influences on the material properties of the final product. Generally, promotion of rutile phase as well as growth in crystallites size with increasing temperature of calcination was observed. In our previous study (Ref 32), it has been shown that rutile phase with relatively small crystallites (ca. 20-60 nm) can be successfully used for mineralization of phenol in water under visible light. Therefore, in the following studies, preparation of rutile-type TiO₂ by sol-gel method was performed with focusing on obtaining of relatively small size crystallites. This is possible by selecting the proper conditions of preparation such as pH, the composition of ingredients, and also calcination temperature and heating rate. Rutile is basically less active than anatase under UV light irradiation, which can be active under visible light, but important is to increase the mobility of induced holes to the photocatalyst surface. This mobility could be improved when the size of rutile crystallites would be reduced and when charge recombination would be retarded. Within the proposed sol-gel method and following calcination some TiO₂/Cu samples were prepared with relatively small crystallites size of rutile. It was proved that addition of Cu prevents against rapid growing of rutile crystals during calcination. Cu can be also electron acceptor and therefore can retard recombination of free carriers

B. Tryba, J. Orlikowski, R.J. Wróbel, J. Przepiórski, and A.W. Morawski, West Pomeranian University of Technology, ul. Pulaskiego 10, 70-322 Szczecin, Poland. Contact e-mail: beata.tryba@zut.edu.pl

after light excitation. Modification of TiO₂ by Cu can additionally reduce the energy of band gap, facilitating activity of this photocatalyst under visible light. The band-gap reduction after modification of TiO₂ with copper can be higher when rutile phase of TiO₂ is present.

In this paper, the sol-gel preparation of TiO₂ doped with Cu is presented. The preparation procedure consists of two steps: sol-gel synthesis followed by the thermal treatment. Cu (NO₃)₂·3H₂O was used as a copper precursor. Two sol-gel solutions at different pH conditions were prepared (pH 3 and 1.5). Such obtained amorphous TiO₂ was submitted to thermal treatment at different temperatures, from 400 to 600 °C for 1 h.

2. Experimental

2.1 Materials

TiP (TTiP, 97.0% purity) purchased from Sigma-Aldrich Chemie GmbH (Germany) was used as TiO₂ precursor. For doping TiO₂ with copper, copper(II) trioxonitrate(V) (99.9% purity) purchased from Poch S.A. (Poland) was added to the sol-gel solution. Nitric acid received from Chempur (Poland) was used for controlling of pH. Phenol of analytical grade purchased from Reactivul Bucuresti (Romania) was used as a model organic pollutant. All the intermediate reagents were used as received, without any extra purification. P-25 titanium dioxide (Evonik, Germany) was used as a commercial reference material.

2.2 Catalysts Preparation

2.2.1 Sol-Gel Synthesis. The sol-gel process was carried out at ambient conditions. Two sol-gel solutions were prepared which differed pH. In the first step, 0.033 g of copper(II) trioxonitrate(V) was diluted in 500 mL of ultrapure water under magnetic stirring (300 rpm). Next 29.7 mL of TiP was diluted with equivalent volume of 2-propanol and 0.1 mL of nitric acid. The obtained transparent solution was slowly dropping into copper(II) trioxonitrate(V) solution. During dropping (ca. 20 min.), mixture was magnetically stirred in air. After dropping, the obtained solution (solution I) was mixed for 2 days, and the white colloidal suspension was obtained with pH equaled about 3. The second sol-gel solution (solution II) was obtained in the same way as solution I but with higher amount of nitric acid used. By this way, transparent solution was obtained, and the measured pH of this sol was about 1.5.

In the second step, the obtained solutions were submitted to the aging process for 4 days in ambient conditions. The aging process was carried out in a dark without any mixing. After that, the solutions were subjected to the heat treatment. For comparison, TiO₂ without addition of any copper salt was also prepared according to these two procedures mentioned above.

2.2.2 Heat Treatment Process. Obtained sol-gel solutions were submitted to evaporation in a vacuum evaporator and then were dried in a drier at 70 °C overnight and subsequently followed calcination at different temperatures, from 400 to 650 °C. The samples were kept at the final temperature for 1 h.

The color of the prepared samples was from white-green to slightly grayish. The samples are identified on the basis of the sol-gel solution type (I and II) and calcination temperature

using the following scheme as an example: I-400-TiO₂/Cu denotes sol-gel solution I and calcination temperature of 400 °C, II-550-TiO₂/Cu denotes sol-gel solution II and calcination temperature of 550 °C, and so on. Similarly, the nomenclature of the samples obtained without copper precursor is as follows: I-400-TiO₂, II-550-TiO₂, and so on.

2.3 Characteristics of the Prepared Photocatalysts

Several methods, including x-ray diffraction (XRD) analysis and UV-Vis/DR spectroscopy, were used to characterize obtained photocatalysts. The XRD patterns were measured with X'Pert PRO diffractometer (Philips), using Cu K α lamp ($\lambda = 1.54439$ Å, 35 kV, 30 mA). in Bragg-Brentano configuration. The Cu K α radiation ($K_{\alpha 1} = 0.154056$ nm; $K_{\alpha 2} = 0.154439$ nm; 35 kV 30 mA) was applied. K_{β} was removed with the filter while $K_{\alpha 2}$ with the numerical procedure of Rachinger's method. The Philips HighScore plus software (Pdf4+ database) was used for phase identification. XRD patterns were measured to determine the average sizes of titania crystallites and to estimate relative phase compositions, i.e., shares of anatase, rutile, and brookite in the prepared photocatalysts. Both, average crystallites size and relative content, were evaluated based on (101), (110), and (211) reflexes for anatase, rutile, and brookite, respectively. The Scherrer formula expressed in Eq 11 was applied (Ref 33):

$$d = \frac{K \cdot \lambda}{(B - b) \cdot \cos \theta}, \quad (\text{Eq 1})$$

where d —the average crystallite size; K —shape factor; λ —x-ray wavelength; B —line width (FWHM) originating both from crystallite sizes and instrumental broadening; b —line width originating solely from instrumental broadening; θ —reflex position.

The shape factor 0.94 was assumed, and the broadening of the reflex is originating solely from instrumental broadening and the size of the crystallites. The instrumental broadening was estimated by the measurement of silicon reference sample for several reflexes and interpolation for anatase (101), rutile (110), and brookite (211) positions.

The percentage content of each phase in the obtained titania powders was calculated using following equation:

$$X_R = \frac{0.41 \cdot I_R}{0.41 \cdot I_R + 0.31 \cdot I_A + I_B} \quad (\text{Eq 2})$$

where X_R —weight fraction of rutile; I_R , I_A , and I_B —integral intensities of rutile (110), anatase (101), and brookite (211) peaks.

The formula was obtained by utilization of reference intensity ratio (RIR) factors from PDF-4+ database. The cards of reference codes 01-088-1172, 01-071-1168, and 01-076-1937 were used for rutile, anatase, and brookite, respectively. If there is no brookite in titania powder, then obtained formula is similar to that one given by Inagaki et al. (Ref 34). However, there is a negligible difference of factors (0.75 versus 0.79).

Quantitative fraction of copper in the photocatalysts was determined by atomic emission spectroscopy with inductively coupled plasma ICP-OES (spectrometer Optima 5300 DV, Perkin Elmer).

Concentration of copper on TiO₂ surface and its binding energy were measured by XPS method. The x-ray photoelectron spectra (XPS) were obtained in a multipurpose three-chamber ultrahigh vacuum (UHV) surface analysis system

(Prevac) operating at base pressures 10-11 mbar range. The sample prior measurement was degassed in vacuum dryer at 100 °C for 24 h. Next the sample was placed as a powder to sample holder. Horizontal transfer of the sample holder during whole procedure enables measurement of powders without special mounting; thus, it eliminates the possibility of appearance of the signals originating from the other than sample sources. The spectra were obtained using Al K α ($h = 1486.6$ eV) radiation with use of Scienta SES 2002 spectrometer operating at constant transmission energy ($E_p = 50$ eV). The substantial charging of the powder was observed. Therefore, correction of binding energy was performed based on titania Ti 2p $_{3/2}$ signal (458.46 eV (Ref 35)).

UV-Vis/DR spectra were recorded using UV-Vis diffuse reflectance spectrophotometer (Jasco V-650, Japan), equipped with an integrating sphere. The band-gap energies were evaluated from the diffuse reflectance data, by plotting of the Kubelka-Munk function, $(F(R)h\nu)^{1/2}$ versus $h\nu$, where R —reflectance, h —Planck constant, ν —frequency, and $F(R) = (1 - R)^2/2R$ (Ref 36-39).

The photocatalytic activity of the prepared samples was investigated for phenol decomposition under visible-light irradiation. The commercial TiO $_2$ P-25 of Evonik company was used as a reference sample. At first, 500 mL of phenol aqueous solution (20 ppm) and 0.1 g of a photocatalyst were loaded into a glass beaker and were agitated with a magnetic stirrer (300 rpm) for 30 min in a dark in order to establish an adsorption/desorption equilibrium. Afterward, the mixtures were irradiated using OSRAM light bulb (60 W) for 24 h. The measured intensity of the reflux light was around 223.5 W/m 2 in the Vis region and 0.18 W/m 2 in UV.

After every 24 h of irradiation, 10 mL of each suspension was filtrated through the 0.45 μ m membrane filter and taken for analyses of total organic carbon (TOC) in multi N/C 3100 analyzer (Analytic Jena Germany).

3. Results and Discussion

3.1 Phase Composition of Photocatalysts and BET Surface Area

XRD patterns collected for all the prepared materials as well as for the commercial P-25 are shown in Fig. 1.

The XRD patterns of the samples synthesized at higher pH (around 3) and calcined at 400 °C (Fig. 1a, I-400-TiO $_2$ /Cu) reveal two coexisted phases of TiO $_2$, anatase, and brookite, whereas in the case of samples calcined at the same temperature but hydrolyzed at lower pH (around 1.5) (Fig. 1b, II-400-TiO $_2$ /Cu) additionally rutile phase of TiO $_2$ appeared. Increase of the calcination temperature to 600 °C led to the increasing in the intensity of anatase peaks (at $2\theta = 25.3^\circ$, 37.7° , and 47.9°) in the samples from Series I but decreasing in case of those from Series II. Transformation of anatase to rutile occurred in the samples from series I at 550 °C simultaneously with increasing intensity of anatase peaks, whereas in case of sample from Series II calcined at 550 °C, rutile phase of TiO $_2$ was dominant. In general, samples calcined from Series II revealed transformation to rutile at lower temperature than in case of Series I and faster disappearance of brookite. Finally, the calcination at 650 °C of sample from Series I (I-650-TiO $_2$ /Cu) resulted in phase mixture of anatase and rutile, while in the case of sample

from Series II (II-650-TiO $_2$ /Cu), the rutile phase existed only. However, XRD analysis did not indicate the presence of any copper phases. Probably the amount of Cu in the prepared TiO $_2$ -samples was out of the detection limit. Similar behavior of phase changing during calcination temperature was observed for both series (I and II) of TiO $_2$ samples prepared without addition of Cu salt. XRD patterns for TiO $_2$ samples itself are not shown here; however, the changes of phase composition of TiO $_2$ and TiO $_2$ -Cu with increasing temperature of calcination are shown in Fig. 2.

From these results, it can be assumed that low pH of sol-gel solution such as pH 1.5 promotes formation of rutile phase of TiO $_2$. These observations are in a good agreement with those reported by the other authors (Ref 40, 41). This mechanism may be explained by using the concept of partial charge model (Ref 42, 43). According to this model, hydrolysis of the titanium cation occurs at low-acidic pH. First, the stable species of $[\text{Ti}(\text{OH})(\text{OH}_2)_5]^{3+}$ are formed in the hydrolysis process under strong acid conditions. However, due to the positive charge of hydroxo group, these species are not able to condense. Moreover, when acidity is not sufficiently low to stabilize these precursors, deprotonation takes place, forming new species of $[\text{Ti}(\text{OH})_2(\text{OH}_2)_4]^{2+}$, which also does not condense. Probably the reason of this fact is spontaneous intramolecular oxolation to $[\text{TiO}(\text{OH}_2)_5]^{2+}$. However, condensation to both anatase and rutile starts when the solution activity is sufficiently high to allow further deprotonation to $[\text{TiO}(\text{OH})(\text{OH}_2)_4]^+$, which can undergo intramolecular deoxolation to $[\text{Ti}(\text{OH})_3(\text{OH}_2)_3]^+$, depending on the exact pH. In the lower pH region, deoxolation does not occur, and oxolation leads to linear growth along the equatorial plane of the cations. This reaction leads to rutile formation, due to oxolation between the resulting linear chains. On the other hand, at higher pH values, when deoxolation takes place, condensation can proceed along apical directions and leads to the skewed chains of the anatase structure. Therefore, based on this study, it is suppose that the determination of resulting crystal phases is affected by pH of sol-gel synthesis and then calcination temperature. With increasing temperature of calcination, the intensity of rutile peaks increases, while the intensity of both anatase and brookite decreases. Calcination at ever higher temperature favors the sintering of anatase crystallites and promotes rutile transformation (Ref 44). Moreover, the disappearance of the peaks assigned to the brookite with an increase of calcination temperature can indicate that brookite also undergoes transformation to the rutile phase, which was reported by the others authors (Ref 45). Therefore, formation of crystalline phase of TiO $_2$ can be controlled by both, the pH of sol-gel synthesis and temperature of calcination. For the sample prepared at the presence of a copper salt at pH solution = 1.5, rutile phase was formed more preferentially during calcination than for TiO $_2$ solution used only. At 500 °C, sample I-500-TiO $_2$ /Cu consisted from almost 80% of rutile, whereas I-500-TiO $_2$ exhibited rutile in the amount of around 20%. However, at pH solution = 3.0 was opposite, Cu retarded phase transformation of anatase onto rutile.

The changes of crystallites size with increasing temperature of calcination are shown in Fig. 3. The interconnecting lines between points depict the trend growth of TiO $_2$ crystallites.

The TiO $_2$ /Cu samples calcined at 400 °C showed crystallites size of anatase around 9.1-9.7 nm. Anatase was growing up with increasing the calcination temperature; however, in case of TiO $_2$ /Cu samples from series II, this growth was partly

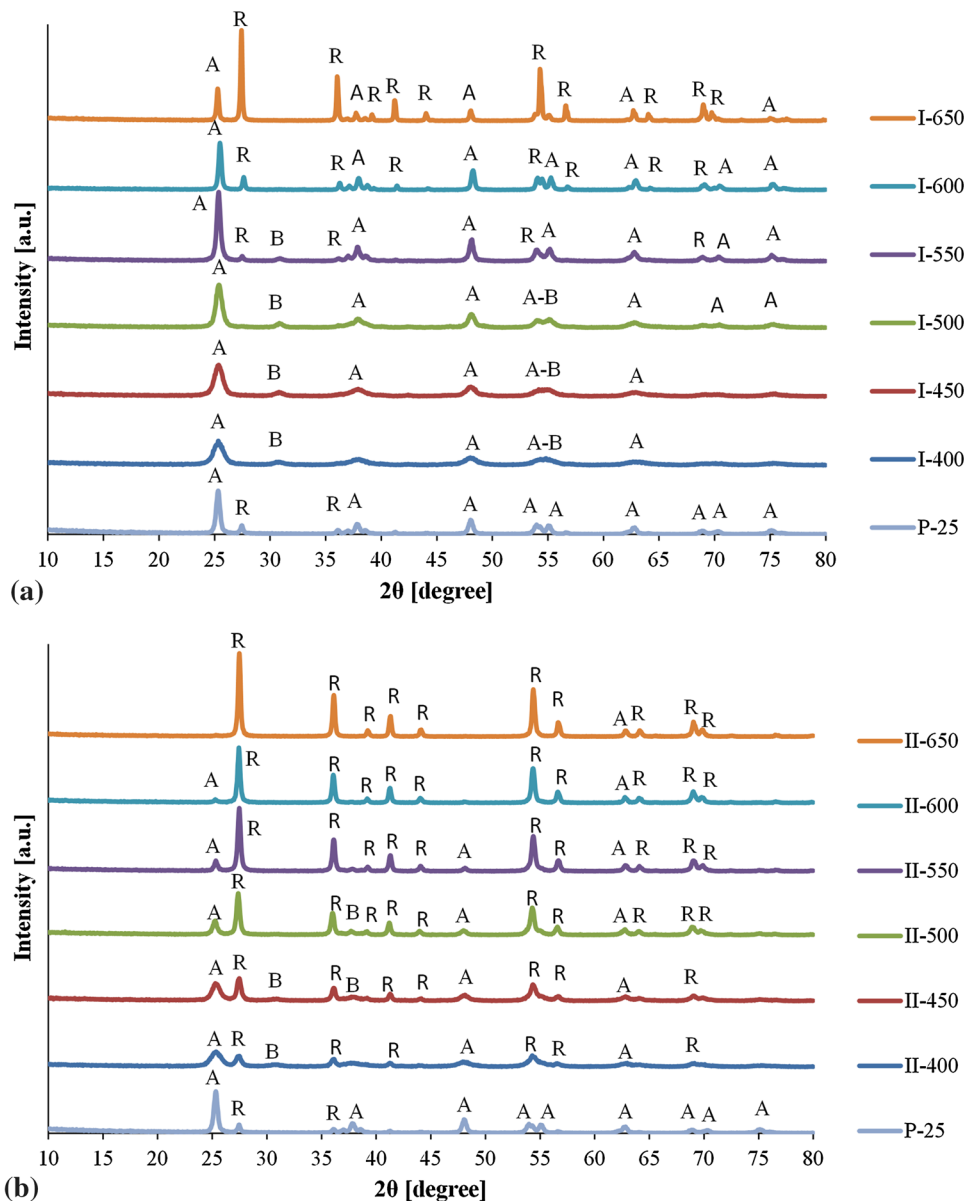


Fig. 1 (Color online) XRD patterns for P-25 and TiO₂/Cu samples of (a) series I and (b) series II, where A—anatase, B—brookite, R—rutile, A-B—anatase peak overlapped with brookite

inhibited due to the fast transformation of anatase to rutile. Therefore, sample I-650-TiO₂/Cu showed average crystallite size of anatase of around 70 nm whereas sample II-650-TiO₂/Cu around 29 nm. Crystallites of rutile appeared in sample II-400-TiO₂/Cu with average size of 20 nm and share of 27%. The share of rutile phase and its crystallites size were gradually increasing with increase of calcination temperature in both series of samples; however, in case of samples from series I (TiO₂/Cu and TiO₂), rutile appeared quantitatively at 600 and 550 °C, respectively, and then its crystallites ambiguously increased reaching around 172 and 160 nm at 650 °C. In case of TiO₂/Cu samples prepared from solution II, the crystallites of rutile were increasing slower, and their average size at 650 °C was 61 nm. The similar results were obtained by the other authors (Ref 46-49).

The amount of copper incorporated into TiO₂ was verified by ICP-OES measurements. Mass fraction (%) of copper in the

selected catalysts of both series is as follows: 0.064, 0.067, and 0.076 for I-400-TiO₂/Cu, I-600-TiO₂/Cu, I-650-TiO₂/Cu and 0.079, 0.081, 0.085, and 0.077 for II-400-TiO₂/Cu, II-550-TiO₂/Cu, II-600-TiO₂/Cu, and II-650-TiO₂/Cu, respectively.

Performed quantitative analyses showed that the amount of copper in the prepared samples was very small, below 1 wt.%. However, the samples synthesized at lower pH (1.5) exhibited somewhat higher amount of copper in comparison to those synthesized at pH 3. Incorporation of Cu in TiO₂ is probably connected with the presence of rutile phase. It is already known that anatase as well as brookite are metastable phases which can be transformed to rutile during heat treatment process. This stable rutile phase has more developed surface defect sites in comparison to the anatase or brookite ones, and therefore, it can successfully attract different dopants, for example, copper.

Insignificantly higher content of Cu in the samples heated at higher temperature in comparison with those calcined at lower

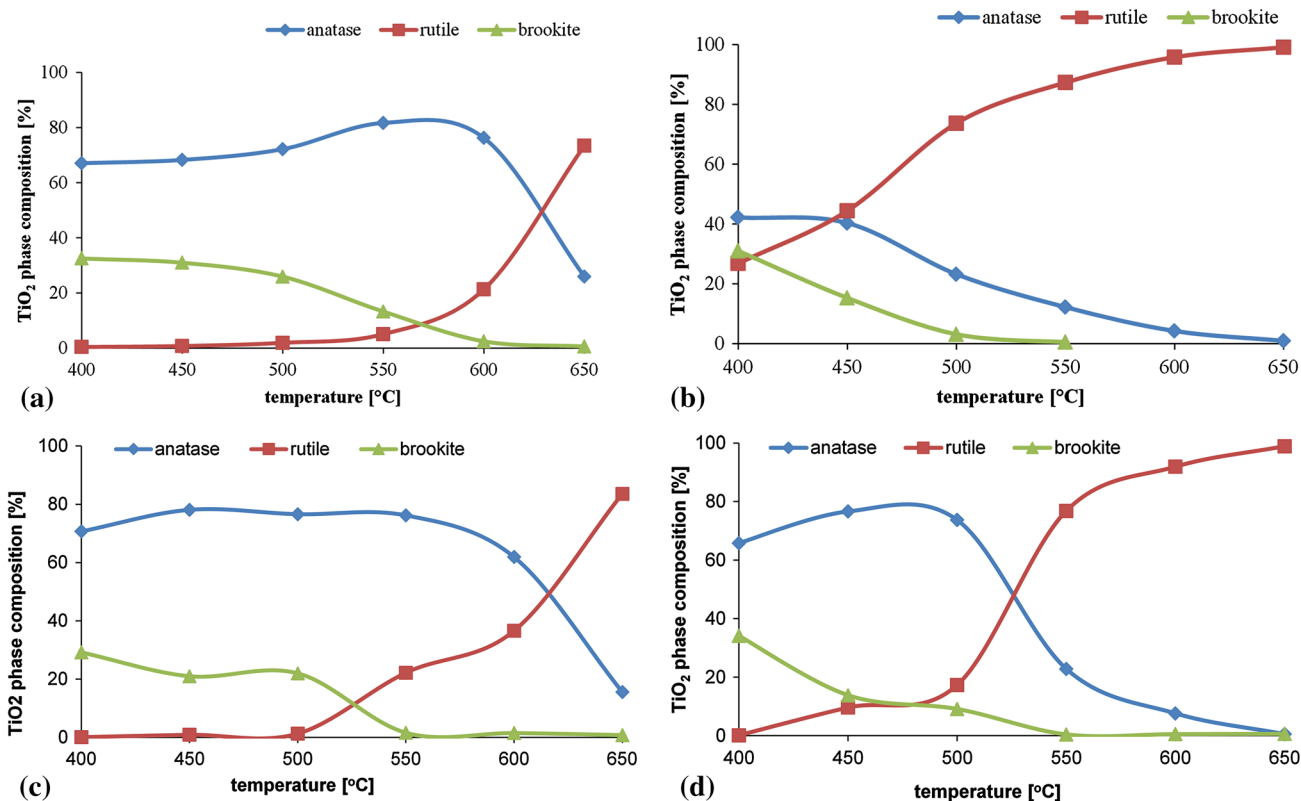


Fig. 2 (Color online) The changes of phase composition with increasing temperature of calcination, (a) TiO_2/Cu —series I, (b) TiO_2/Cu —series II, (c) TiO_2 —series I, and (d) TiO_2 —series II

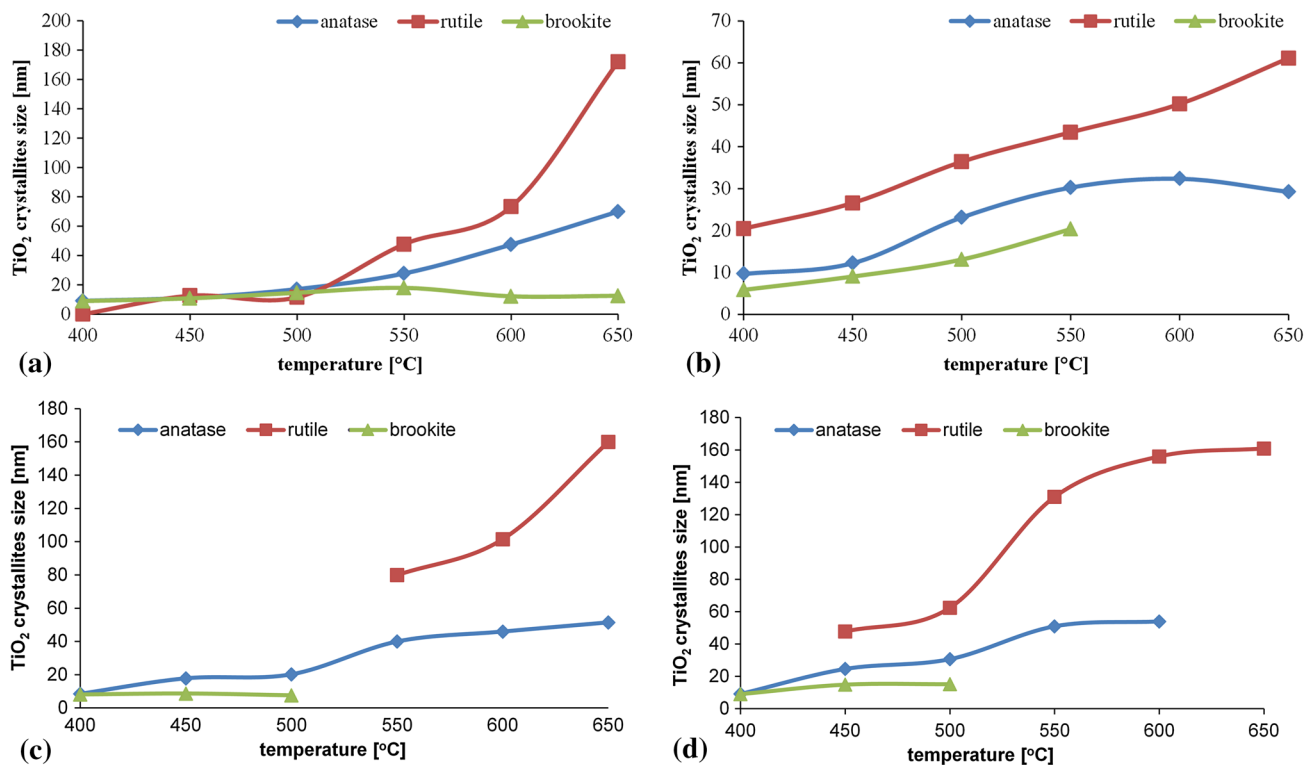


Fig. 3 (Color online) The changes of crystallites size with increasing temperature of calcination, (a) TiO_2/Cu —series I, (b) TiO_2/Cu —series II, (c) TiO_2 —series I, and (d) TiO_2 —series II

one was connected with decreasing the content of organic compounds during burning. Thus, the total mass of sample was reduced, and then the share of copper was higher.

BET surface area was measured for some of TiO_2/Cu samples. For the sample I-400- TiO_2/Cu , BET surface area was $130.3 \text{ m}^2/\text{g}$, whereas for II-400- TiO_2/Cu , BET surface area was much lower, only $68.8 \text{ m}^2/\text{g}$. It is connected with the crystallites size: the former one consisted with the average crystallites size for all the phases below 20 nm, whereas the latter one had already rutile crystallites, over 20 wt.% with an average size around 20 nm. During calcination process, the crystallites were growing up, and as a consequence, BET surface area was reduced; for I-500- TiO_2/Cu sample, it was estimated to be $16.8 \text{ m}^2/\text{g}$ and for II-500- TiO_2/Cu — $12.9 \text{ m}^2/\text{g}$, whereas for these samples heated at $550 \text{ }^\circ\text{C}$, it was even lower, 9.8 and $9.9 \text{ m}^2/\text{g}$ for I-550- TiO_2/Cu and II-550- TiO_2/Cu , respectively.

3.2 XPS Measurements

In Fig. 4, the XPS spectra are presented for sample I-600- TiO_2/Cu . The surface concentration of copper is 0.4 or 1.1 wt.%. It is more than determined by ICP method and

indicates that copper is located over surface of titania. The poor signal to noise ratio in case of Cu 2p spectrum is a result of very low concentration of Cu in the sample. The position of Cu $2p_{3/2}$ signal is 932.4 eV. This can be attributed to either Cu^{1+} (932.18 eV, Ref 1), or Cu^0 state (932.63 eV, Ref 35; 932.7 eV, Ref 50). The Cu^{2+} (933.76 eV, Ref 35) can be excluded because of lack of shake-up signals' characteristic for CuO or $\text{Cu}(\text{OH})_2$ compounds. Signal O 1s was at 530.0 eV what is in excellent agreement with the literature data (Ref 35).

3.3 UV-Vis/DR Spectroscopy

The UV-Vis/DR spectra measured for obtained and P-25 reference sample together with band-gap energies calculated using the Kubelka-Munk reemission function are shown in Fig. 5.

Based on the UV-Vis/DR spectra of the samples of both series, listed in Fig. 5, the changes in the adsorption spectra with increase of calcination temperature can be noticed. It is found that with increasing calcination temperature, the adsorption in the visible region increased. Additionally, the red shifting of the adsorption edge took place resulting in the

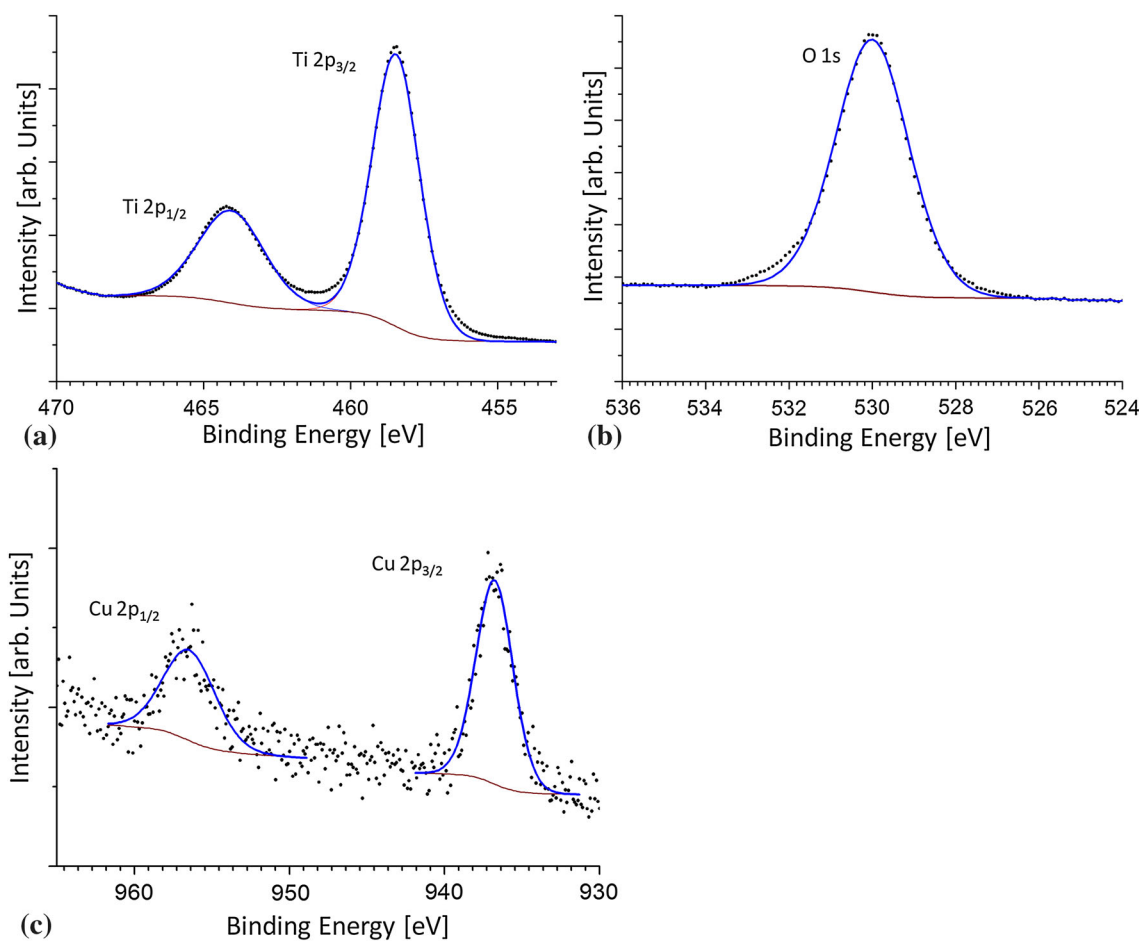


Fig. 4 XPS spectra of I-600- TiO_2/Cu sample. Relatively high noise in case of Cu 2p signal is result of low copper concentration

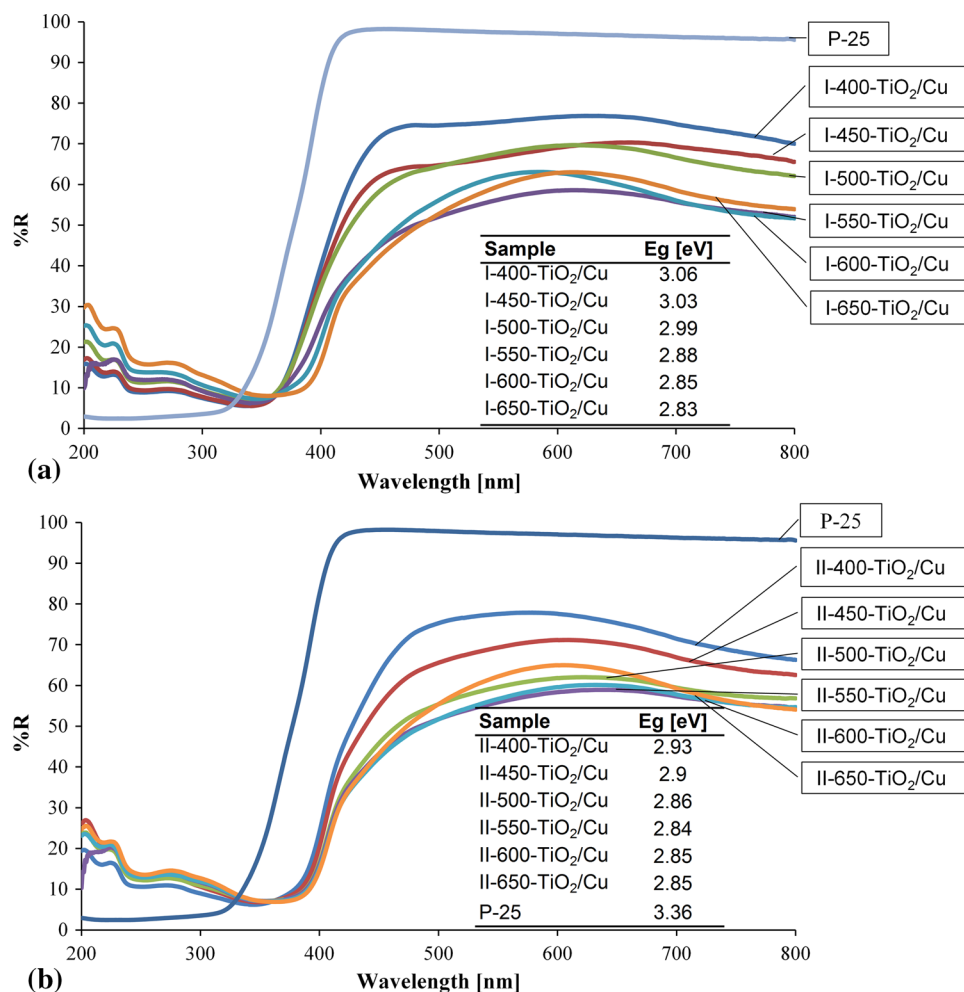


Fig. 5 UV-Vis/DR spectra and band-gap energies of P-25 and prepared TiO₂ photocatalysts of: (a) TiO₂/Cu—series I, (b) TiO₂/Cu—series II, (c) TiO₂—series I, and (d) TiO₂—series II, where R —lights reflectance, E_g —band-gap energy evaluated by the Kubelka-Munk function

decrease in the value of the band-gap energy. The most dynamic changes in the adsorption edge as well as in reducing the energy of the band gap were observed between TiO₂/Cu samples of series I calcined at 500 and 550 °C, whereas in case of TiO₂/Cu samples of series II, the same changes were observed between samples calcined at 450 and 500 °C. For TiO₂ samples, reduction of the band-gap energy with increasing calcination temperature was also observed but to lower value than it was observed for TiO₂/Cu series. According to the literature (Ref 51-53), the shifting of the adsorption edge as well as the decreasing value of band-gap energy can be related to the changes in the phase composition of TiO₂. Rutile phase has lower energy of the band-gap than anatase and brookite; therefore, at the presence of rutile, the red shifting of the adsorption edge was higher. Additionally, doping Cu to TiO₂ causes shifting of the absorption edge to the higher values (Ref 54, 55). All the prepared samples revealed two advantages in

comparison to P-25: higher adsorption in the visible region and the red shifting of the absorption edge.

3.4 Photodegradation of Phenol

Adsorption of phenol after an establishing adsorption-desorption equilibrium and photocatalytic mineralization of phenol after 24 h of visible-light irradiation on prepared samples and P-25 are presented in Fig. 6.

The adsorption ability of TiO₂ photocatalysts toward phenol is increasing with increasing calcination temperature, and it is higher for samples consisted with rutile and Cu. Thus, the TiO₂/Cu samples of series II calcined at 600 and 650 °C had the highest adsorption capacity among the other samples. It can be deduced that at the absence of Cu, higher adsorption of phenol occurs on the rutile phase. In the literature, it can be found that P-25 adsorbs phenol in the quantity of 53 μmol/g (Ref 56);

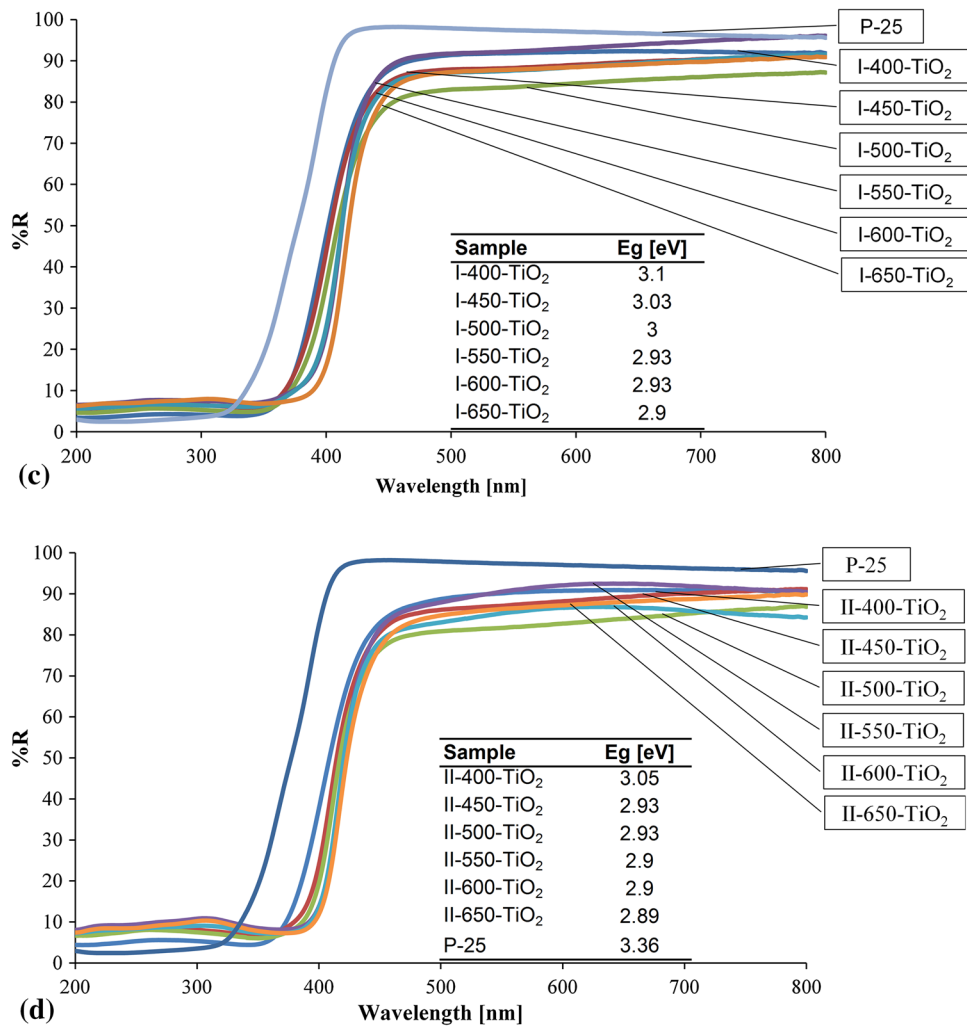


Fig. 5 continued

however, in these studies, the adsorption of phenol on P-25 was not noticed. It can be caused by the shorter time of adsorption process carried out in these measurements than in the other ones, before reaching adsorption maximum. On the TiO₂ samples prepared by sol-gel method, the quantitative adsorption occurred within 1 h, and the same time was kept for all the measured samples. Maybe for P-25, this time was not enough to reach adsorption-desorption equilibrium. Mineralization of phenol was somewhat higher on the TiO₂/Cu samples than TiO₂, calcined at higher temperature, such as 600 and 650 °C (II-600-TiO₂/Cu and I-650-TiO₂/Cu). These

samples exhibited low energy of the band gap, $E_g = 2.83$ and 2.85 eV, respectively. These low values of E_g were caused by both, the presence of rutile and incorporation of Cu. The presence of Cu on TiO₂ surface is beneficial because it increases adsorption abilities toward phenol, can retard recombination by the possible electron scavenging, and also reduces band-gap energy of rutile enabling visible-light activation. Preparation of TiO₂/Cu at low pH such as 1.5 causes formation of rutile at early stages, and then its calcination at 600 °C is effective for making photocatalyst active under visible light.

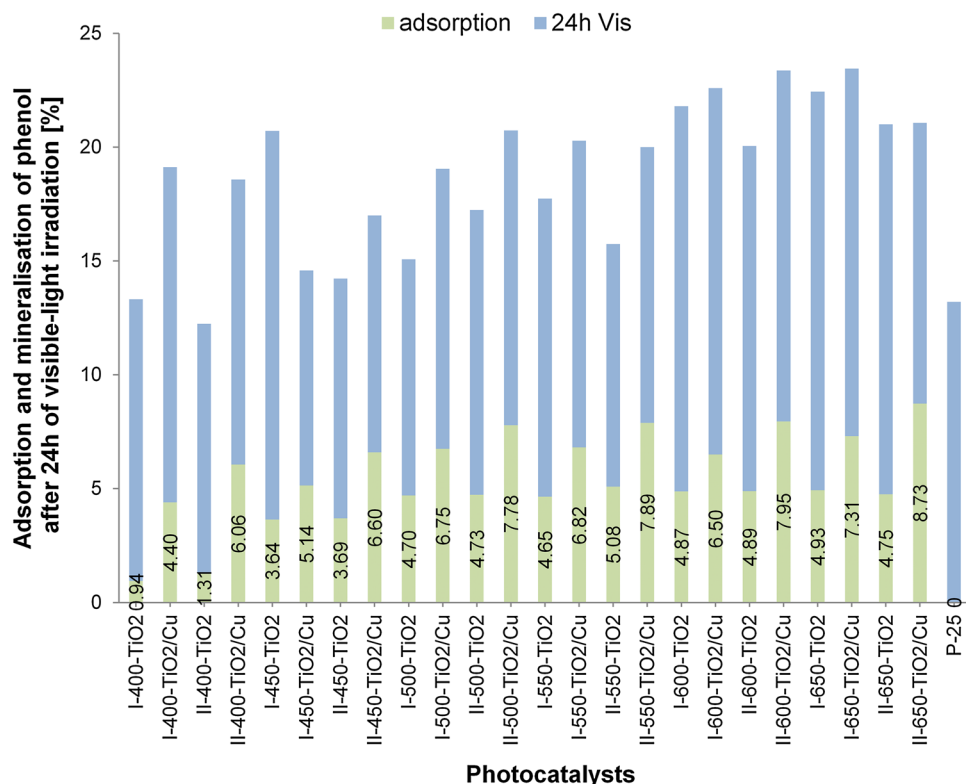


Fig. 6 (Color online) Adsorption of phenol after an establishing adsorption-desorption equilibrium and photocatalytic mineralization of phenol after 24 h of visible-light irradiation on P-25 and the prepared photocatalysts

4. Conclusions

Low pH of sol-gel solution (1.5) favors formation of rutile during calcination and causes faster transformation of brookite to rutile within increasing of heat treatment temperature. This effect is enhanced at the presence of copper salt. At this low pH of sol-gel the particles of TiO_2/Cu are more stabilized than at higher pH and sol-gel without Cu because with increasing calcination temperature, there is observed the gradual growth of rutile and anatase, whereas at pH = 3, above 500 °C, these crystallites start to grow rapidly.

Doping Cu to TiO_2 caused shifting the absorption edge to the visible region and significant reduction of band-gap energy. This effect was more noticeable at higher temperature of calcination, in case of solution I (pH = 3) ≥ 550 °C, at lower pH of sol-gel solution (pH = 1.5), when temperature was ≥ 500 °C.

Photocatalytic degradation of phenol was more effective on rutile-type TiO_2 doped with Cu, which revealed low energy of band gap (2.83-2.85 eV) and relatively high adsorption of phenol in comparison to other samples. Preferential location of Cu on TiO_2 surface-enhanced photocatalytic activity of rutile under visible light.

Open Access

This article is distributed under the terms of the Creative Commons Attribution License which permits any use, distribution, and reproduction in any medium, provided the original author(s) and the source are credited.

References

1. L. Chiodo, M. Salazar, A. Romero, S. Laricchia, F. Della Sala, and A. Rubio, Structure, Electronic, and Optical Properties of TiO_2 Atomic Clusters: An Ab Initio Study, *J. Chem. Phys.*, 2011, **135**, p 244704
2. P. Roy, S. Berger, and P. Schmuki, TiO_2 Nanotubes: Synthesis and Applications, *Angew. Chem. Int. Ed.*, 2011, **50**, p 2904–2939
3. W. Choi, Pure and Modified TiO_2 Photocatalysts and Their Environmental Applications, *Catal. Surv. Asia*, 2006, **10**, p 16–28
4. Y. Park, S.-H. Lee, S.O. Kang, and W. Choi, Organic Dye-Sensitized TiO_2 for the Redox Conversion of Water Pollutants Under Visible Light, *Chem. Commun.*, 2010, **46**, p 2477–2479
5. A. Orlov, M.S. Chan, D.A. Jefferson, D. Zhou, R.J. Lynch, and R.M. Lambert, Photocatalytic Degradation of Water-Soluble Organic Pollutants on TiO_2 Modified with Gold Nanoparticles, *Environ. Technol.*, 2006, **27**, p 747–753
6. S.G. Kumar and L.G. Devi, Review on Modified TiO_2 Photocatalysis Under UV/Visible Light: Selected Results and Related Mechanisms on Interfacial Charge Carrier Transfer Dynamics, *J. Phys. Chem. A*, 2011, **115**, p 13211–13241
7. P. Roy, D. Kim, K. Lee, E. Spieckerb, and P. Schmuki, TiO_2 Nanotubes and Their Application in Dye-Sensitized Solar Cells, *Nanoscale*, 2010, **2**, p 45–59
8. H. Zhang, G. Du, W. Lu, L. Cheng, X. Zhu, and Z. Jiao, Porous TiO_2 Hollow Nanospheres: Synthesis, Characterization and Enhanced Photocatalytic Properties, *Cryst. Eng. Commun.*, 2012, **14**, p 3793–3801
9. J. Lu, Y. Dai, M. Guo, L. Yu, K. Lai, and B. Huang, Chemical and Optical Properties of Carbon-Doped TiO_2 : A Density-Functional Study, *Appl. Phys. Lett.*, 2012, **100**, p 102114–102117
10. X. Chen and C. Burda, The Electronic Origin of the Visible-Light Absorption Properties of C-, N- and S-Doped TiO_2 Nanomaterials, *J. Am. Chem. Soc.*, 2008, **130**, p 5018–5019
11. Y. Park, W. Kim, H. Park, T. Tachikawa, T. Majima, and W. Choi, Carbon-Doped TiO_2 Photocatalyst Synthesized Without Using an External Carbon Precursor and the Visible Light Activity, *Appl. Catal. B*, 2009, **91**, p 355–361

12. J. Yu, S. Liu, Z. Xiu, W. Yu, and G. Feng, Synthesis of Sulfur-Doped TiO₂ by Solvothermal Method and Its Visible-Light Photocatalytic Activity, *J. Alloys Compd.*, 2009, **471**, p 23–25
13. U.G. Akpan and B.H. Hameed, The Advancements in Sol–Gel Method of Doped-TiO₂ Photocatalysts, *Appl. Catal. A*, 2010, **375**, p 1–11
14. T.K. Tseng, Y.S. Lin, Y.J. Chen, and H. Chu, A Review of Photocatalysts Prepared by Sol-Gel Method for VOCs Removal, *Int. J. Mol. Sci.*, 2010, **11**, p 2336–2361
15. T.V. Anuradha and S. Ranganathan, Nanocrystalline TiO₂ by Three Different Synthetic Approaches: A Comparison, *Bull. Mater. Sci.*, 2007, **30**, p 263–269
16. S. Lee, C.Y. Yun, M.S. Hahn, J. Lee, and J. Yi, Synthesis and Characterization of Carbon-Doped Titania as a Visible-Light-Sensitive Photocatalyst, *Korean J. Chem. Eng.*, 2008, **25**, p 892–896
17. M. Guo and J. Du, First-Principles Study of Electronic Structures and Optical Properties of Cu, Ag, and Au-Doped Anatase TiO₂, *Physica B*, 2012, **407**, p 1003–1007
18. H. Diker, C. Varlikli, K. Mizrak, and A. Dana, Characterizations and Photocatalytic Activity Comparisons of N-Doped nc-TiO₂ Depending on Synthetic Conditions and Structural Differences of Amine Sources, *Energy*, 2011, **36**, p 1243–1254
19. M. Sahu and P. Biswas, Single-Step Processing of Copper-Doped Titania Nanomaterials in a Flame Aerosol Reactor, *Nanoscale Res. Lett.*, 2011, **6**, p 441
20. V. Blaskov, M. Shipochka, I. Stambolova, S. Vassilev, A. Eliyas, P. Stefanov, and A. Loukanov, Influence of Titanium Precursor on the Photocatalytic Properties of TiO₂ Sprayed Films Under Visible Light, *J. Phys. Conf. Ser.*, 2012, **398**, p 012021
21. S. Preda, V.S. Teodorescu, A.M. Musuc, C. Andronescu, and M. Zaharescu, Influence of the TiO₂ Precursors on the Thermal and Structural Stability of Titanate-Based Nanotubes, *J. Mater. Res.*, 2013, **28**, p 294–303
22. C. Mailhe-Randolph, A.J. McEvoy, and M. Grätzel, Influence of Precursors on the Morphology and Performance of TiO₂ Photoanodes, *J. Mater. Sci.*, 1991, **26**, p 3305–3308
23. X. Bokhimi, O. Novaro, R.D. Gonzalez, T. López, O. Chimal, A. Asomoza, and R. Gómez, Copper Precursor Effect on Reducibility and Titania Phases Concentration of Sol-Gel Cu/TiO₂ Catalyst, *J. Solid State Chem.*, 1999, **144**, p 349–353
24. Z.S. Pap, L. Baia, K. Mogyorósi, A. Dombi, A. Oszkó, and V. Danciu, Correlating the Visible Light Photoactivity of N-Doped TiO₂ with Brookite Particle Size and Bridged-Nitro Surface Species, *Catal. Commun.*, 2012, **17**, p 1–7
25. S. Livraghi, M.C. Paganini, M. Chiesa, and E. Giamello, Trapped Molecular Species in N-Doped TiO₂, *Res. Chem. Intermed.*, 2007, **33**, p 739–747
26. I.H. Tseng, J.C.S. Wu, and H.Y. Chou, Effects of Sol-Gel Procedures on the Photocatalysis of Cu/TiO₂ in CO₂ Photoreduction, *J. Catal.*, 2004, **221**, p 432–440
27. H.W.P. Carvalho, M.V.J. Rocha, P. Hammer, and T.C. Ramalho, TiO₂-Cu Photocatalysts: A Study on the Long- and Short-Range Chemical Environment of the Dopant, *J. Mater. Sci.*, 2013, **48**, p 3904–3912
28. X. Bokhimi, A. Morales, and O. Novaro, Effect of Copper Precursor on the Stabilization of Titania Phases, and the Optical Properties of Cu/TiO₂ Prepared with the Sol-Gel Technique, *Chem. Mater.*, 1997, **9**, p 2616–2620
29. A. Yin, X. Guo, K. Fan, and W.-L. Dai, Influence of Copper Precursors on the Structure Evolution and Catalytic Performance of Cu/HMS Catalysts in the Hydrogenation of Dimethyl Oxalate to Ethylene Glycol, *Appl. Catal. A*, 2010, **377**, p 128–133
30. M.A. Santana-Aranda, M. Morán-Pineda, J. Hernández, and S. Castillo, Physical Properties of TiO₂ Prepared by Sol-Gel Under Different pH Conditions for Photocatalysis, *Superficies y Vacío*, 2005, **18**(1), p 46–49
31. A. Karami, Synthesis of TiO₂ Nano Powder by the Sol-Gel Method and Its Use as a Photocatalyst, *Iran. Chem. Soc.*, 2010, **7**, p S154–S160
32. J. Orlikowski, B. Tryba, J. Ziebro, A.W. Morawski, and J. Przepiórski, A New Method for Preparation of Rutile Phase Titania Photoactive Under Visible Light, *Catal. Commun.*, 2012, **24**, p 5–10
33. A.L. Patterson, The Scherrer Formula for X-ray Particle Size Determination, *Phys. Rev.*, 1939, **56**, p 978–982
34. M. Inagaki, R. Nonaka, B. Tryba, and A.W. Morawski, Dependence of Photocatalytic Activity of Anatase Powders on Their Crystallinity, *Chemosphere*, 2006, **64**, p 437–445
35. M.C. Biesinger, L.W.M. Lau, A.R. Gerson, and R.St.C. Smart, Resolving Surface Chemical States in XPS Analysis of First Row Transition Metals, Oxides and Hydroxides: Sc, Ti, V, Cu and Zn, *Appl. Surf. Sci.*, 2010, **257**, p 887–898
36. S. Mozia, A. Heciak, and A.W. Morawski, The Influence of Physicochemical Properties of TiO₂ on Photocatalytic Generation of C₁–C₃ Hydrocarbons and Hydrogen from Aqueous Solution of Acetic Acid, *Appl. Catal. B*, 2011, **104**, p 21–29
37. A.B. Murphy, Band-Gap Determination from Diffuse Reflectance Measurements of Semiconductor Films, and Application to Photoelectrochemical Water-Splitting, *Sol. Energy Mater. Sol. Cells*, 2007, **91**, p 1326–1337
38. S. Valencia, J.M. Marin, and G. Restrepo, Study of the Bandgap of Synthesized Titanium Dioxide Nanoparticles Using the Sol-Gel Method and a Hydrothermal Treatment, *Open Mater. Sci. J.*, 2010, **4**, p 9–14
39. I. Tunc, M. Bruns, H. Gliemann, M. Grunze, and P. Koelsch, Bandgap Determination and Charge Separation in Ag@TiO₂ Core Shell Nanoparticle Films, *Surf. Interface Anal.*, 2010, **42**, p 835–841
40. J.-P. Nikkanen, T. Kanerva, and T. Mäntylä, the Effect of Acidity in Low-Temperature Synthesis of Titanium Dioxide, *J. Cryst. Growth*, 2007, **304**, p 179–183
41. H. Cheng, J. Ma, Z. Zhao, and L. Qi, Hydrothermal Preparation of Uniform Nanosize Rutile and Anatase Particles, *Chem. Mater.*, 1995, **7**, p 663–671
42. S.T. Aruna, S. Tirosh, and A. Zaban, Nanosize Rutile Titania Particle Synthesis Via a hydrothermal Method Without Mineralizers, *J. Mater. Chem.*, 2000, **10**, p 2388–2391
43. R. Reisfeld, Chemistry, Spectroscopy and Applications of Sol-Gel Glasses, *Structure and Bonding*, R. Reisfeld and C.K. Jorgensen, Ed., Springer, New York, 1992, p 153–206
44. D.A.H. Hanaor and C.C. Sorrell, Review of the Anatase to Rutile Phase Transformation, *J. Mater. Sci.*, 2011, **46**, p 855–874
45. S. Bakardjieva, V. Stengl, L. Szatmary, J. Subrt, J. Lukac, N. Murafa, D. Niznansky, K. Cizek, J. Jirkovsky, and N. Petrova, Transformation of Brookite-Type TiO₂ Nanocrystals to Rutile: Correlation Between Microstructure and Photoactivity, *J. Mater. Chem.*, 2006, **16**, p 1709–1716
46. M. Hamadani, A. Reisi-Vanani, and A. Majedi, Synthesis, Characterization and Effect of Calcination Temperature on Phase Transformation and Photocatalytic Activity of Cu, S-Codoped TiO₂ Nanoparticles, *Appl. Surf. Sci.*, 2010, **256**, p 1837–1844
47. P. Górska, A. Zaleska, E. Kowalska, T. Klimczuk, J.W. Sobczak, E. Skwarek, W. Janusz, and J. Hupka, TiO₂ Photoactivity in Vis and UV light: The Influence of Calcination Temperature and Surface Properties, *Appl. Catal. B*, 2008, **84**, p 440–447
48. D.A.H. Hanaor and C.C. Sorrell, Review of the Anatase to Rutile Phase Transformation, *J. Mater. Sci.*, 2011, **46**, p 855–874
49. T. Miki, K. Nishizawa, E. Watanabe, and H. Taoda, Effect of Calcination Temperature on the Microstructure of Porous TiO₂ Film, *Res. Chem. Intermed.*, 2009, **35**, p 257–262
50. J. Przepiórski, A.W. Morawski, and A. Oya, Method for Preparation of Copper-Coated Carbon Material, *Chem. Mater.*, 2003, **15**, p 862–865
51. D. Reyes-Coronado, G. Rodriguez-Gattorno, M.E. Espinosa-Pesqueira, C. Cab, R. de Coss, and G. Oskam, Phase-Pure TiO₂ Nanoparticles: Anatase, Brookite and Rutile, *Nanotechnology*, 2008, **19**, p 145605–145615
52. J.G. Li, T. Ishigaki, and X.J. Sun, Anatase, Brookite, and Rutile Nanocrystals Via Redox Reactions Under Mild Hydrothermal Conditions: Phase-Selective Synthesis and Physicochemical Properties, *Phys. Chem. C*, 2007, **111**, p 4969–4976
53. W.J. Yin, S.Y. Chen, J.H. Yang, X.G. Gong, Y.F. Yan, and S.H. Wei, Effective Band Gap Narrowing of Anatase TiO₂ by Strain Along a Soft Crystal Direction, *Appl. Phys. Lett.*, 2010, **96**, p 221901
54. Z. Liu, Y. Wang, X. Peng, Y. Li, Z. Liu, C. Liu, J. Ya, and Y. Huang, Photoinduced Superhydrophilicity of TiO₂ Thin Film with Hierarchical Cu Doping, *Sci. Technol. Adv. Mater.*, 2012, **13**, p 025001
55. H.W. Slamet, E. Nasution, K. Purnama, and J. Riyani, Gunlazuardi Effect of Copper Species in a Photocatalytic Synthesis of Methanol from Carbon Dioxide over Copper-Doped Titania Catalysts, *World Appl. Sci. J.*, 2009, **6**, p 112–122
56. A. Turki, C. Guillard, F. Dapozze, Z. Ksibi, G. Berhault, and H. Kochkar, Phenol Photocatalytic Degradation over Anisotropic TiO₂ Nanomaterials: Kinetic Study, Adsorption Isotherms and Formal Mechanisms, *Appl. Catal. B*, 2015, **163**, p 404–414